

## Supporting Information

### **Highly integrated all-in-one electrochromic fabrics towards unmanned environmental adaptive camouflage**

*Guoxing Fu<sup>a,#</sup>, Hui Gong<sup>a,#</sup>, Jinheng Xu<sup>b</sup>, Biying Zhuang<sup>a</sup>, Baoli Rong<sup>a</sup>, Qianqian Zhang<sup>a,\*</sup>, Xiaoqing Chen<sup>b,\*</sup>, Jingbing Liu<sup>a</sup>, Hao Wang<sup>a,\*</sup>*

*<sup>a</sup>Key Laboratory for New Functional Materials of Ministry of Education, Faculty of Materials and Manufacturing, Beijing University of Technology, Beijing 100124, P. R. China.*

*<sup>b</sup>Key Laboratory of Optoelectronics Technology, Ministry of Education, Faculty of Information Technology, Beijing University of Technology, Beijing 100124, China.*

### **Content of Supporting Information**

1. The FTIR spectra of the PANI electrode
2. The cross-sectional SEM images of the all-in-one ECF
3. The manufacturing process of traditional EC fabrics
4. The CV curves of PANI electrodes at different polymerization charges
5. The SEM of PANI at different polymerization charges
6. The optical testing of PANI at different polymerization charges
7. The bending performance of the all-in-one ECF
8. The SEM images of PANI and Al after flattening and bending of the all-in-one ECF
9. The electrochromic behavior of the all-in-one ECF attaching on various polyhedron surfaces.
10. The all-in-one ECF of environmental adaptive camouflage system
11. The HLS value of PANI electrodes
12. The response time of the PANI electrode
13. Comparison of the performance of other EC devices
14. References

## 1. The FTIR spectra of the PANI electrode

As shown in Fig. S1, PANI exhibited obvious absorption peaks at 850  $\text{cm}^{-1}$ , 1010  $\text{cm}^{-1}$ , 1160  $\text{cm}^{-1}$ , 1363  $\text{cm}^{-1}$ , 1461  $\text{cm}^{-1}$ , and 1538  $\text{cm}^{-1}$ . The peak around at 1538  $\text{cm}^{-1}$  was assigned to the C=C stretching vibrations of quinoid ring.<sup>1</sup> The peaks appeared at 1461  $\text{cm}^{-1}$  and 1363  $\text{cm}^{-1}$  corresponded to the stretching mode of benzene ring and C–N stretching mode.<sup>2</sup> The peak at the 1160  $\text{cm}^{-1}$  was the formation of  $-\text{NH}^+=$  vibrations from the quinone structure  $-\text{N}=\text{}$  in polyaniline by protonation. The peaks at 1010  $\text{cm}^{-1}$  and 850  $\text{cm}^{-1}$  correspond to the in-plane and out-of-plane bending of the C-H group, respectively.<sup>3</sup>

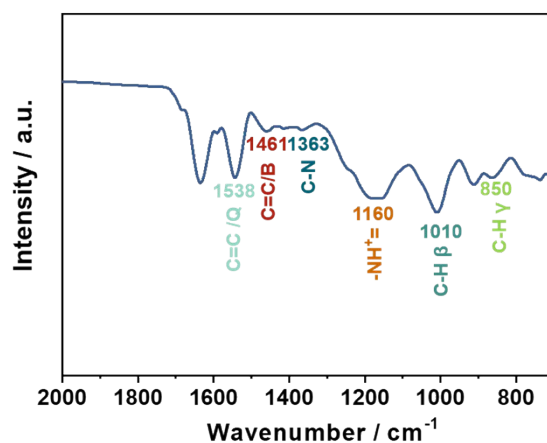


**Fig. S1.** The FTIR spectra of the PANI electrode. Inset shows the molecular structure of PANI

## 2. The cross-sectional SEM images of the all-in-one ECF

As shown in Fig. S2, each layer was uniform and had a tight adhesion with others according to the element distributions from the cross-section, which further suggested the high integration of the all-in-one ECF. The mapping element analysis showed the delamination between the different layers. Therefore, the short circuit could be effectively avoided by controlling the thickness of the gold and aluminum layers.

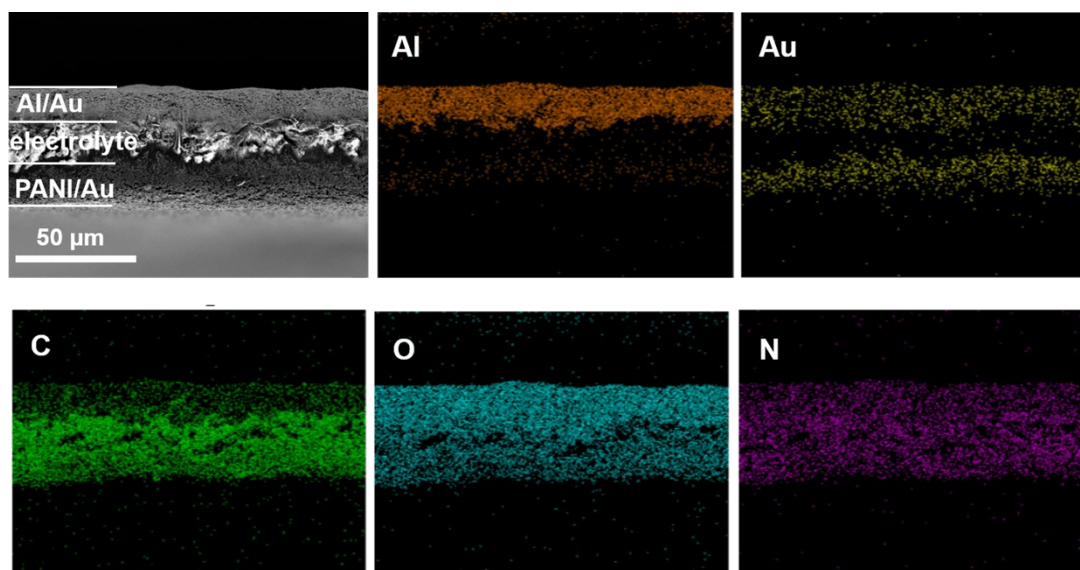


**Fig. S2.** The cross-sectional SEM images of the all-in-one ECF and the corresponding elemental mapping of each layer.

### 3. The manufacturing process of traditional EC fabrics

The schematic illustration of the fabrication process of the traditional EC fabric was exhibited in Fig.S3. The PANI films and Al layer was deposited on the two side of Au/nylon membrane, respectively, which were used as the EC and counter electrodes. The  $\text{AlCl}_3$  ( $1 \text{ mol L}^{-1}$ ) gel electrolyte was filled in nylon membrane by vacuum filtration method.

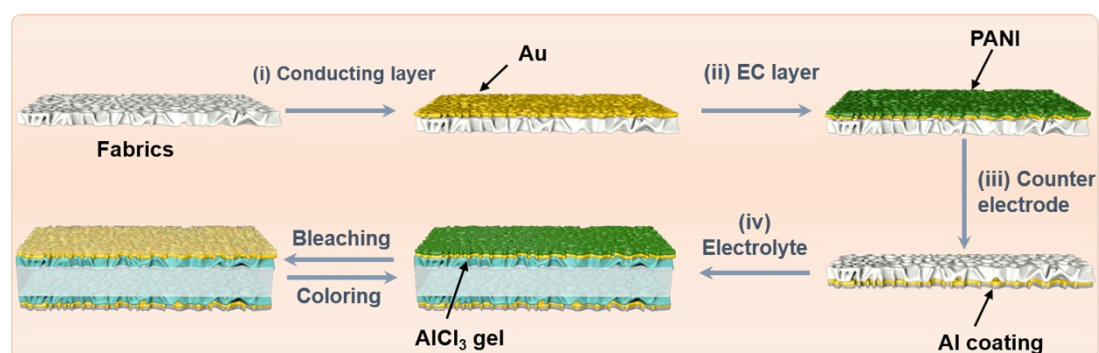
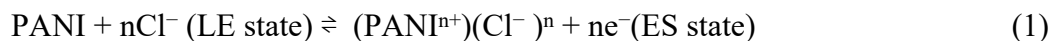


**Fig. S3.** The schematic illustration of the fabrication procedure of the traditional EC fabric based on the PANI electrodes.

#### 4. The CV curves of PANI electrodes at different polymerization charges

The reduction peak potential and oxidation peak potential represent the leucoemeraldine (LE) state of PANI and emeraldine salt (ES) state, the transformation between the ES and LE state is caused by  $\text{Cl}^-$  anion doping and dedoping, the overall redox reaction equation is as follows<sup>4,5</sup>:



As shown in Fig. S4, the CV curves of the as-prepared PANI electrodes with different polymerization charges revealed that the closed area of the CV curve of electrodes became larger with the polymerization charges increasing from 0.5 C to 4.0 C. In addition, the resistance of PANI electrodes increased as the polymerization charge increasing, which result in the positive shift of the oxidation peak and a negative shift of the corresponding reduction peak.

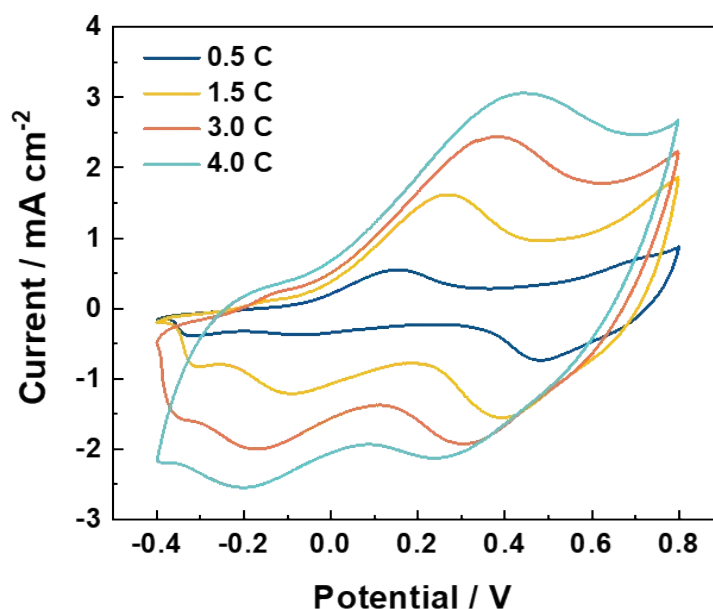


**Fig. S4.** The CV curves of the PANI electrodes at different polymerization charges measured in  $1 \text{ mol L}^{-1} \text{ AlCl}_3$  aqueous solution with a scan rate of  $20 \text{ mV s}^{-1}$ .

## 5. The SEM of PANI at different polymerization charges

The SEM images of PANI electrodes at different polymerization charges also analysed in Fig. S5. Noted that Au/nylon membranes were gradually covered by PANI film with the increasing of polymerization charges. Meanwhile, the content of PANI film on the porous membranes gradually increased as the polymerization charge increasing.

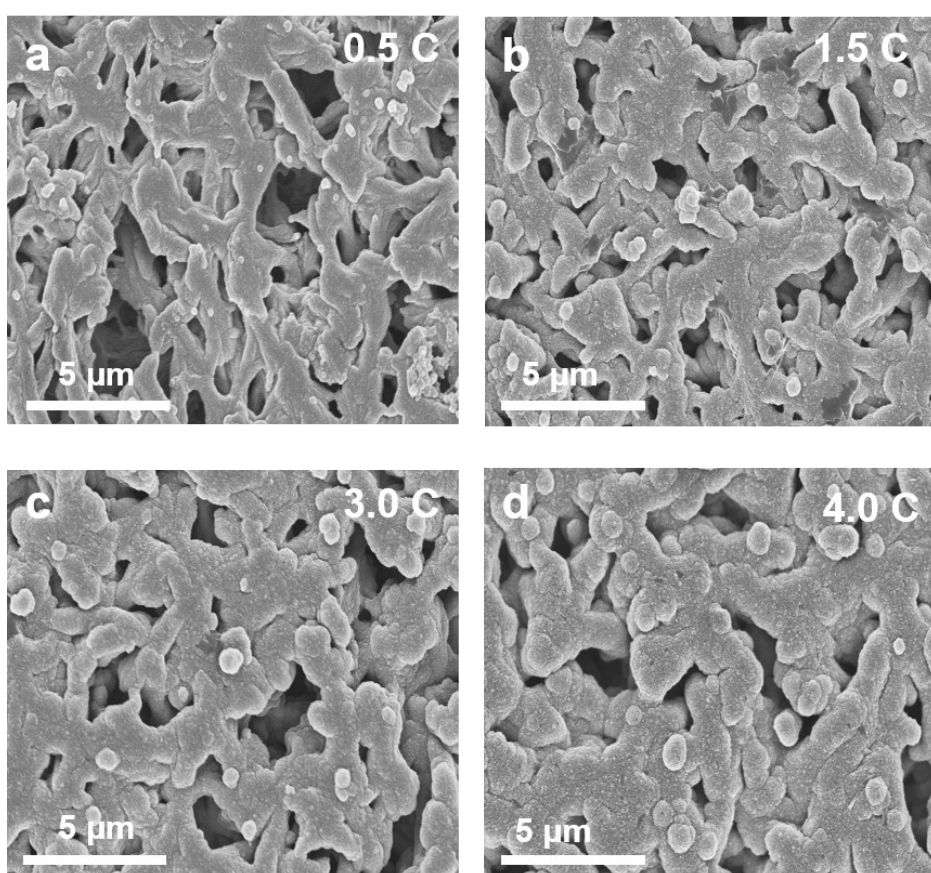


**Fig. S5.** The SEM images of PANI electrodes at 0.1 mA/cm<sup>2</sup> with polymerization charges from 0.5 C to 4.0 C. (a) 0.5 C (b) 1.5 C (c) 3.0 C (d) 4.0 C

## 6. The optical testing of PANI at different polymerization charges

As shown in Fig. S6, the CIE color coordinates of PANI with different polymerization charges showed multiple blue colors series under oxidation potentials. As shown in Fig. S7, all the Vis-NIR reflectance spectra of PANI at different voltages showed blue shift of the reflection peak. In addition, the response time of the PANI at different voltages were shown in Fig. S8. It can be seen that the response time increases with the increase of polymerization charges, which could be attributed to that more active load makes the occurrence of redox reaction time increase. As demonstrated in Fig. S9, the  $\Delta R$  at 1500 nm increased to 15.1% with 1.5 C due to the increased loading of active PANI on the electrode. And then the  $\Delta R$  decreased when the polymerization charges increased to 3.0 C. The excessive growth of the PANI layer hinders the ion diffusion within the material, resulting in the incomplete redox reaction. Therefore, the optimum polymerization charge to obtain the maximum reflectivity modulation was determined to be 1.5 C.

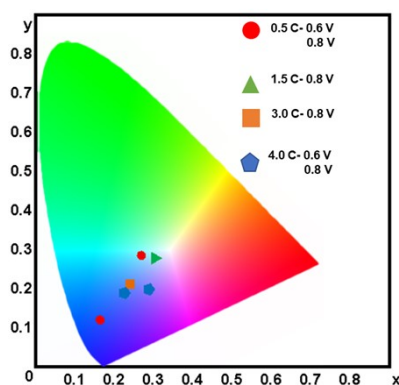


**Fig. S6.** CIE color coordinates of the PANI with different polymerization charges.

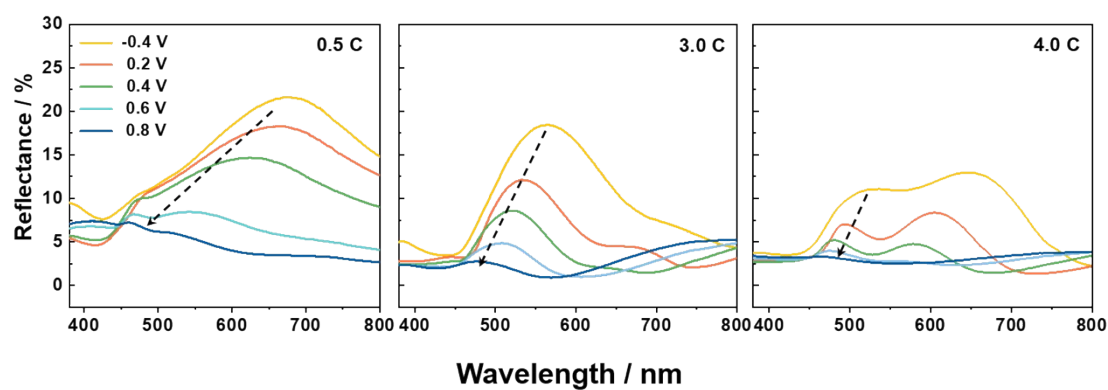


**Fig. S7.** The Vis–NIR reflectance spectra of the PANI electrode at various voltages from  $-0.4$  to  $0.9$  V [vs. Ag/AgCl (sat. KCl)] with polymerization charges increasing from  $0.5$  C to  $4.0$  C.

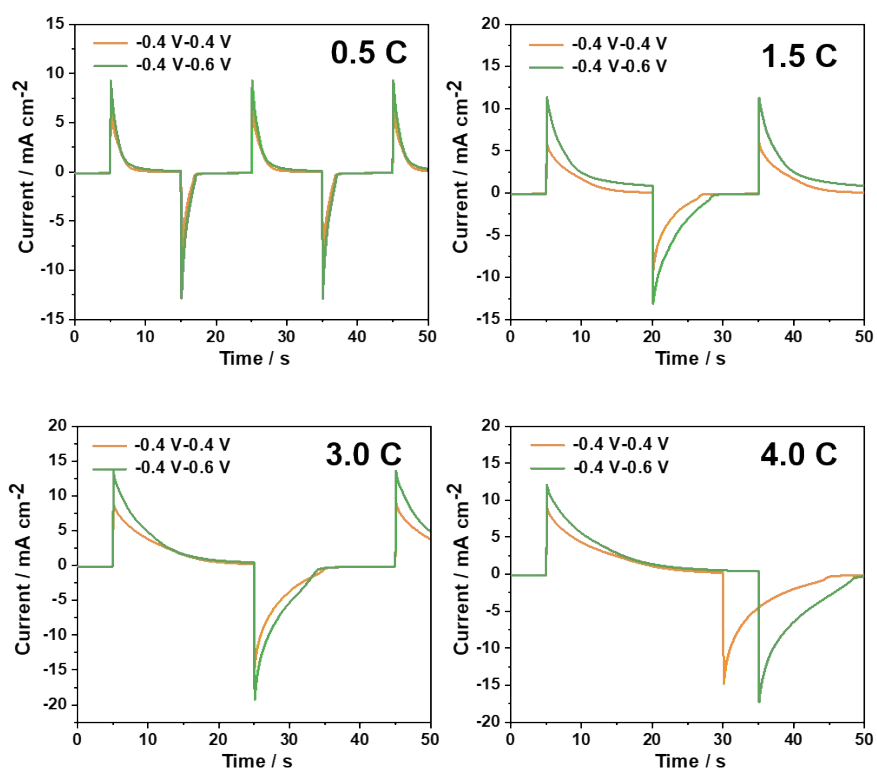


**Fig. S8.** The response time of the PANI electrode at different voltages.

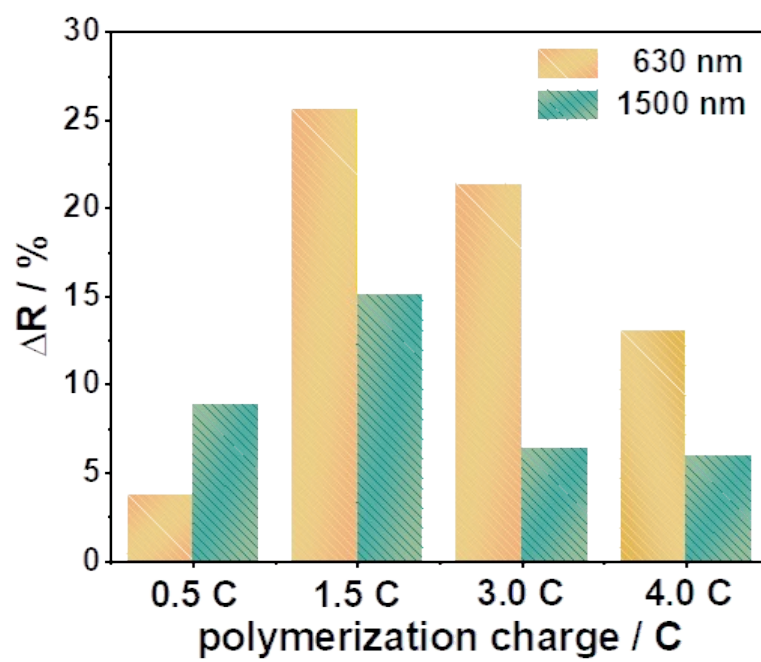


**Fig. S9.** The  $\Delta R$  between the oxidation and reduction states of the electrode at 630 nm and 1500 nm.

## 7. The bending performance of the all-in-one ECF

The bending performance of the all-in-one ECF was further measured by Ocean Spectrometer shown in Fig. S10. As shown in Fig. S11, we further recorded the reflectance spectra of the ECF when the incident light illuminated the sample with different curvatures. The result indicates that ECF still shows the obvious EC behavior under different curvatures.

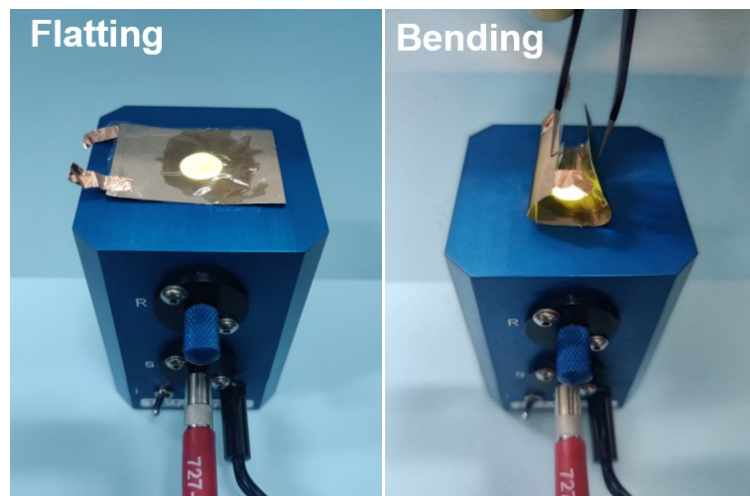


**Fig. S10.** The optical photographs of the all-in-one EFC measured by Ocean Spectrometer.

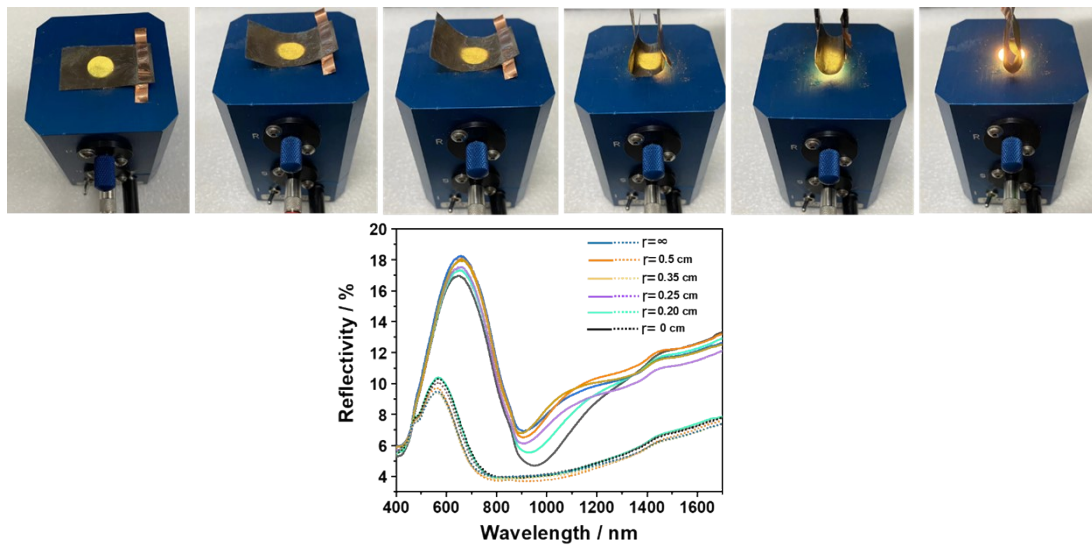


**Fig. S11.** The photographs of the ECF with different curvatures and the corresponding reflectance spectrum.

**8. The SEM images of PANI and Al after flatting and bending of the all-in-one ECF**

As illustrated in Fig. S12, the SEM images of PANI and Al after flatting and bending of the all-in-one ECF, which shows nearly no change in the microstructure of PANI and Al layer after bending 1000 cycles.

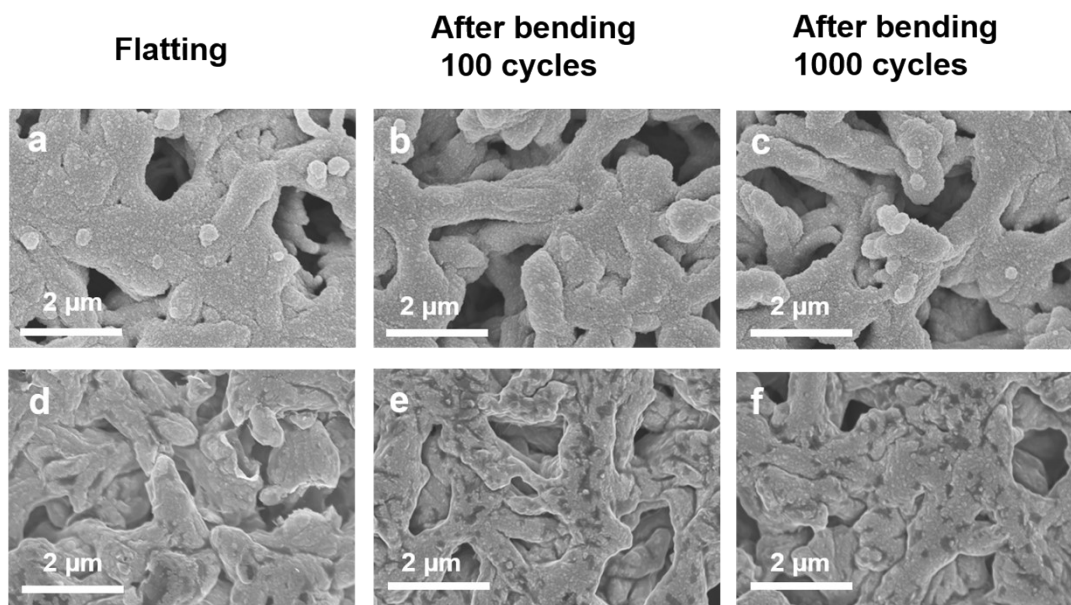


**Fig. S12.** SEM images of PANI (Top) and Al (Bottom): (a) unbending (b) after bending 100 cycles (c) after bending 1000 cycles.

9. The electrochromic behavior of the all-in-one ECF attaching on various polyhedron surfaces.

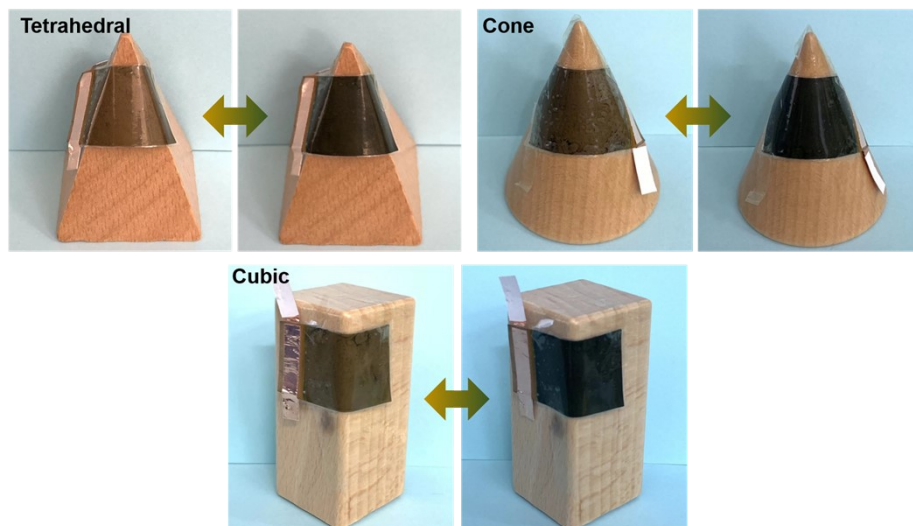


**Fig. S13.** The conformability of the all-in-one ECF with arbitrary surfaces.

## 10. The all-in-one ECF of environmental adaptive camouflage system

As shown in Fig. S14, the artificial camouflage system developed in this work consists of four parts. The part 1 is a RGB color sensor (TCS230) that integrates with a photodiode arrays and a current-to-frequency converter, which can be used to drive TTL or CMOS (Complementary Metal Oxide Semiconductor) of standard. The sensor can achieve the RGB digital signals from the environment color and input it to the microcontroller (Part 2). Then, logical algorithm program can be downloaded into microcontroller (STC89C52) through Keil5 programmer. Finally, voltage AD (Analog-digital-Converter) conversion system in the PCF8591 (Part 3) can convert RGB values to the required stable voltages, ranging from 0 V to 5 V. The output voltages can apply to the electrochromic module (Part 4).

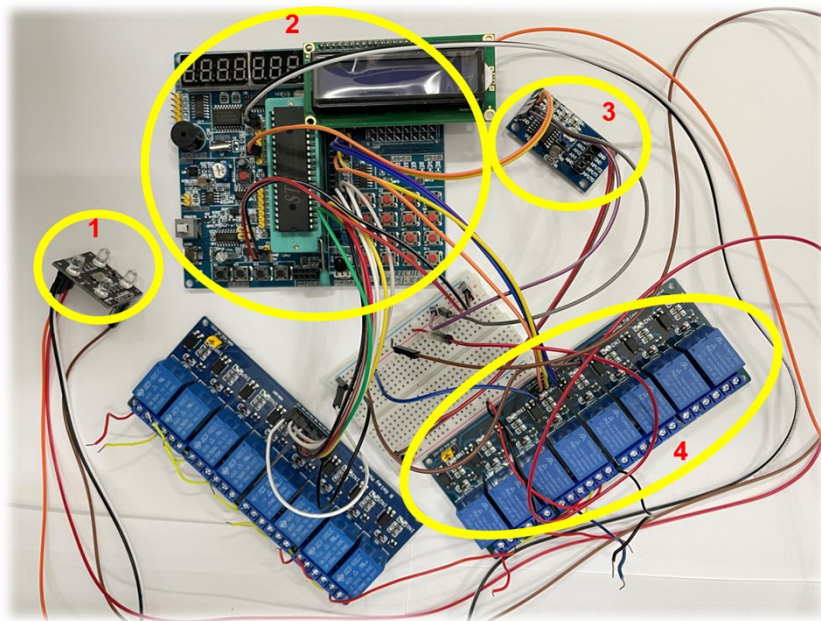


**Fig. S14.** Optical images of environment color monitoring photodiode arrays, logical algorithm program (STC89C52) and an AD converter (PCF8591) of the unmanned environmental adaptive camouflage system.

## 11. HLS value of PANI electrodes

Table S1 HLS value of PANI electrodes at various potentials from -0.4 to 0.8 V [vs Ag/AgCl (sat. KCl)] with polymerization charges from 0.5 C to 4.0 C

**Table S1.** The  $\Delta R$  values of the PANI electrodes with different polymerization charges.

<b>0.5 C</b>	H	L	S
-0.4 V	27.69	45.29	16.88
0.2 V	45.00	36.86	23.40
0.4 V	45.00	34.51	15.91
0.6 V	120.00	28.63	1.37
<b>1.5 C</b>	H	L	S
-0.4 V	40.73	38.63	55.33
0.2 V	48.79	30.78	57.96
0.4 V	68.14	27.25	42.45
0.6 V	157.89	16.67	67.06
<b>3.0 C</b>	H	L	S
-0.4 V	57.43	31.76	43.21
0.2 V	73.77	27.25	43.88
0.4 V	118.24	23.53	28.33
0.6 V	167.78	10.59	100.00
<b>4.0 C</b>	H	L	S
-0.4 V	24.44	36.08	29.35
0.2 V	35.71	27.06	30.43
0.4 V	124.62	20.59	12.38
0.6 V	246.00	13.73	14.29

## 12. The response time of the PANI electrode

The response time of the PANI electrode with polymerization charges from 0.5 C to 4.0 C at different voltages were shown in Table S2.

**Table S2.** The response time of the PANI electrodes at different voltages.

Charges	0.5 C	1.5 C	3.0 C	4.0 C
-0.4-0.4 V	2.7/1.8 s	7.4/9.0 s	12.5/9.0 s	16.4/12.7 s
-0.4-0.6 V	3.7/2.0 s	11.3/7.6 s	16.5/9.5 s	20.6/13.1 s

### 13. Comparison of the performance of other EC devices

**Table S3.** Comparison of the performance of other EC devices

Electrochromic materials/devices	Thickness ( $\mu\text{m}$ )	$\Delta R_{\text{max}}$ (%)	Flexibility	Thermal management	Ref
NBR/PEO/PEDO T semi-IPN	~84.7	16% at 2.5 $\mu\text{m}$	N/A	N/A	6
CPs/IL/CPs	~100	N/A	N/A	N/A	7
PE/H <sub>2</sub> SO <sub>4</sub> -PANI/ P(VDF-HFP)/ H <sub>2</sub> SO <sub>4</sub> -PANI	>200	~6.5% at 2 $\mu\text{m}$	100	9.1 °C	8
PANI-based fiber	906.3	N/A	500	5.0 °C	9
H <sub>2</sub> SO <sub>4</sub> -doped PANI/AlCl <sub>3</sub> gel/Al	>300	21.6 % at 1500 nm	50	5.6 °C	3
All-in-one electrochromic fabric	80	22% at 1500 nm	1000	4.9 °C	This work

## 14. References

1. Gong, H. et al. A self-patterning multicolor electrochromic device driven by horizontal redistribution of ions. *Sol. Energy Mater. Sol. Cells* **2020**, *215*, 110642.
2. Zhang, L. et al. Further understanding of the mechanisms of electrochromic devices with variable infrared emissivity based on polyaniline conducting polymers. *J. Mater. Chem. C* **2019**, *7*, 9878-9891.
3. Gong, H. et al. Self-Driven Infrared Electrochromic Device with Tunable Optical and Thermal Management. *ACS Appl. Mater. Interfaces* **2021**, *13*, 50319-50328.
4. Zhou, K. et al. Polyaniline films with modified nanostructure for bifunctional flexible multicolor electrochromic and supercapacitor applications. *Chem. Eng. J.* **2018**, *345*, 290-299.
5. Zhang, H. et al. Highly stable flexible transparent electrode via rapid electrodeposition coating of Ag-Au alloy on copper nanowires for bifunctional electrochromic and supercapacitor device. *Chem. Eng. J.* **2020**, *399*, 125075.
6. Laurent, J. Goujon et al. Soft and flexible Interpenetrating Polymer Networks hosting electroreflective poly(3,4-ethylenedioxythiophene). *Sol. Energy Mater. Sol. Cells* **2014**, *127*, 33-42.
7. P, Chandrasekhara. et al. Variable Emittance Skins for Active Thermal Control in Spacecraft Based on Conducting Polymers, Ionic Liquids and Specialized Coatings. *J. Appl. Polym. Sci.* **2014**, *131*, 40850.
8. Xu, G. et al. A visible-to-infrared broadband flexible electrochromic device based polyaniline for simultaneously variable optical and thermal management. *Sol. Energy Mater. Sol. Cells* **2020**, *208*, 110356.
9. Liu, D. et al. Fiber-shaped dynamic thermal radiation-regulated device based on

carbon fiber and polyaniline. *Sol. Energy Mater. Sol. Cells* **2022**, *245*, 111855.